

**Complexity signatures in the geomagnetic H-component recorded
by the Tromsø magnetometer (70°N, 19°E) over the last quarter
of a century**

C. M. Hall, Tromsø Geophysical Observatory, University of Tromsø, Norway

Abstract. Solar disturbances, depending on the orientation of the interplanetary magnetic field, typically result in perturbations of the geomagnetic field as observed by magnetometers on the ground. Here, the geomagnetic field's horizontal component, as measured by the ground-based observatory-standard magnetometer at Tromsø (70°N, 19°E) is examined for signatures of complexity. 25 year-long 10s resolution datasets are analysed, but for fluctuations with timescales less than 1 day. Quantile-quantile plots are employed first, revealing the fluctuations are better represented by Cauchy rather than Gaussian distributions. Thereafter, both spectral density and detrended fluctuation analysis methods are used to estimate values of the generalized Hurst exponent, α . The results are then compared with independent findings. Inspection and comparison of the spectral and detrended fluctuation analyses reveals that timescales between 1h and 1d are characterized by fractional Brownian motion with a generalized Hurst exponent of ~ 1.4 whereas including timescales as short as 1 min suggests fractional Brownian motion with a generalized Hurst exponent of ~ 1.6 . This is consistent with changes in the strength and position of the auroral electrojet that can be considered rapid during the course of an evening, whereas from minute-to-minute the electrojet moves more persistently in geomagnetic latitude.

25 1. Introduction and methodology

Understanding the coupling mechanisms between various processes and phenomena in the solar-Terrestrial system remains a considerable challenge. An approach that has gained popularity in recent years involves examining the noise in a signal (or time-series), i.e. the stochastic rather than the deterministic component. The underlying idea is that a signature in
30 the noise occurring in a driving mechanism may re-appear in the noise of another observable, thus linking the two. This approach is akin to fingerprinting a crime scene. Examination of time series for such fingerprints was pioneered by, inter alios, *Hurst*, [1951], *Mandelbrot*, [1983], *Grassberger and Procaccia*, [1983] and *Koscielny-Bunde et al.* [1998]. Work by *Eichner et al.* [2003] and *Lennartz and Bunde* [2009] and *Kantelhardt et al.* [2006], for
35 example have refined the approach. Much attention has been given to oceanographic and meteorological observables including the recent study by *Hall* [2014], and more recently solar-related observables, e.g. *Scafetta and West* [2003] and *Rypdal and Rypdal* [2011]. On the other hand, there has been relatively little focus on observables related to the terrestrial ionosphere and measured locally in order to examine the mapping of solar forcing to the
40 Earth's surface. *Hall et al.* [2011] examined complexity in the ionospheric E-region in the auroral zone: the altitude, strength and persistence of the E-region are of particular interest for radio communications and for studying the possible overall shrinking of the middle atmosphere due to climatic cooling [*Roble and Dickinson*, 1989; *Rishbeth and Clilverd*, 1999]. In this particular study, the geomagnetic field characteristics represented by a local
45 time series measured, on average, beneath the auroral oval at 70°N 19°E (geographic), will be examined. Stochastic variations appear as fluctuations driven by ionospheric currents and thus associated magnetic fields perturbing the background geomagnetic field. The time series employed will be described in more detail forthwith.

The approach to analysing the geomagnetic field data here is the same as that used by *Hall* [2014]: first the data are filtered using a boxcar to remove all periodicities less than one day and the result is then subtracted from the original time series, thus producing a residual excluding all pre-conceived (deterministic) periodicities. This is equivalent to “deseasonalization” commonly applied to neutral atmosphere data, for example. The reasoning for removing all fluctuations of period 1 day or larger will become apparent when the data are described in more detail.

The majority of studies to obtain complexity signatures from time series aim at evaluating the Hurst exponent, H , as invented by *Hurst*, [1951] as a quantification of the scaling nature, or self-affinity of the stochastic component of the data. H , however lies in the interval $\{0,1\}$ and alone cannot identify the process as fractional Gaussian noise (fGn) or fractional Brownian motion (fBm) as invented by *Mandelbrot and van Ness* [1968]. In the concept of fBm successive increments are correlated: the time series is non-stationary and with temporally varying variance fGn, on the other hand, is stationary and time-invariant in expectation value and variance. In these processes, positive correlation between successive increments indicates that preceding motion is likely to continue and negative correlation indicates that preceding motion is likely to be followed by a reversal, likelihoods commonly referred to as persistent and anti-persistent, respectively. Rather than derive H , therefore, the approach of *Kantelhardt et al.* [2006] is adopted here and the *generalized Hurst exponent*, α , is derived. The two exponents are related: for fGn, $H = \alpha$ and for fBm, $H = \alpha - 1$. Thus, α unambiguously characterizes as process as fBm ($\alpha > 1$), persistent fGn ($0.5 < \alpha < 1$) and anti-persistent fGn ($0 < \alpha < 0.5$), with $\alpha = 1.5$ indicating the special case of Brownian motion. Furthermore, one can define the scaling exponent of the power spectrum of the signal (the negative of the spectral slope in log-log space) by β :

$$S(f) \propto |f|^{-\beta} \quad (1)$$

White noise is thus characterized by a flat spectrum and therefore $\beta=0$. “Pink noise” is when $\beta=1$, and the case where $\beta=2$ is referred to as “red noise” and corresponds to Brownian motion, e.g. *Vasseur and Yodzis* [2004]. Importantly, the *generalized Hurst exponent*, α and the power spectrum scaling exponent, β are related by

$$\alpha = (\beta + 1)/2 \quad (2)$$

as explained by, e.g., *Hartmann et al.* [2013], and *Delignieres et al.* [2006], and references therein. The relationship is conveniently summarized in Figure 1 of *Hall* [2014]. Moreover, the fractal or Hausdorff-Besicovich dimension, $D = 2 - H$, but assuming *fBm*. One can see, therefore, calculating D by, for example, the method of *Grassberger and Procaccia*, [1983], can potentially yield H but not unambiguously provide the same information as α .

Following the sequence used by *Hall* [2014], rather than blindly launch into a determination of α which will almost inevitably yield some result, the data are examined first for indications of non-linearity by inspections of the probability density function (PDF) and quantile-quantile (Q-Q) analyses [*Wilk and Gnanadesikan*, 1968]. A PDF can indicate qualitatively if the distribution is non-Gaussian. In Q-Q plots, quantiles of the distribution of the noise in the signal are plotted against those derived from a semi-empirical Gaussian distribution having the same mean and standard deviation; a straight line will result if the signal exhibits a Gaussian distribution. With a preconception of the nature of the PDF a number of approaches may be employed to obtain α . Some of the most used methods are described and compared by *Delignieres et al.* [2006], *Hartmann et al.* [2013] and *Heneghan and McDarby* [2000] (note, however, that these last authors use “ α ” as the spectral scaling exponent rather than β). Using experience gained from *Hall* [2014] α is obtained using both spectral analysis (SA) and

detrended fluctuation analysis (DFA); while most physicists will feel comfortable with the
 95 more intuitive SA, DFA [Peng *et al.* 1993] is arguably the preferred method in contemporary
 research when searching for long-term memory in data. For the purposes of SA, since
 experimental data are under consideration, the time series should be treated as irregularly
 sampled; data gaps are few, but even so must be assumed to exist. Lomb-Scargle
 periodogram analysis [Press and Rybicki, 1989] is more appropriate than a Fourier transform.
 100 Additionally, Fougère [1985] and Eke *et al.* [2000] have proposed preconditioning of the
 time series by applying a parabolic window, bridge detrending using the first and last points
 in the series, and finally frequency selection prior to attempting to obtain a spectral exponent.
 Applying frequency selection to the Lomb-Scargle periodogram is somewhat unpredictable
 as discovered by Hall [2014], so the entire spectrum is retained. Finally the spectrum S is
 105 plotted vs. f in log-log space to hopefully identify a regime exhibiting a scaling exponent β
 according to Eq.1. In DFA, the stochastic component of the original time series is first
 cumulatively summed (each new point is the sum of the preceding points in the original).
 This cumulative summation is then divided into sub-series of equal length (n). Each of these
 sub-series is then detrended either by subtracting the straight line between end-points (bridge
 110 detrending) or linear or polynomial fits (referred to as DFA(1), DFA(2) etc). Variances are
 calculated for each sub-series and the then averaged to obtain a mean $F(n)$. After repeating
 for a range of sub-series lengths (usually all possible n), the function $F(n)$. is plotted vs. n in
 log-log space (as was done in the spectral analysis case) to hopefully identify a regime
 exhibiting a scaling exponent α :

$$F(n) \propto n^\alpha \quad (3)$$

115 wherein α is the generalized Hurst exponent.. Here, a simple linear detrending will be used
 and DFA will be used to refer to DFA(1).

2. Underlying data and analysis

Analyses of geomagnetic time-series are few relative to for other observables such as surface air temperature (SAT) and, at the other end of the solar-terrestrial system, sunspot number (SSN). Downloadable datasets such as the auroral electrojet index (*AE*) have been examined, e.g. *Rypdal and Rypdal* [2011], but the *AE* index is really a synthesis of individual magnetometer measurements at a selection of observatories under or near the auroral oval. The index is the width of the envelope of north-south geomagnetic field perturbations obtained from typically > 10 stations [e.g. Davis and Sugiura1966]. *Wanliss and Reynolds* [2003] have determined β for a number of low latitude records although references therein accentuate the preceding focus on global indices. *Hamid et al.* [2009] similarly examine data from specific sites. The nature of the data used in this study is somewhat different to those used by *Wanliss and Reynolds* [2003] and *Hamid et al.* [2009], however. The geomagnetic field is usually (but not exclusively) defined by three components: declination, D ($^{\circ}$), horizontal, H (nT), and vertical, Z (nT). When constructing geomagnetic indices as indicators of activity, for example the k -index [*Bartels et al.*, 1939], the horizontal component is preferred because an approximately zonally aligned current system induces a maximum perturbation in the horizontal component of the background field immediately below it. The vertical component, on the other hand induces a zero crossing in the perturbation. The magnetometer at Tromsø (70°N, 19°E) is operated as an observatory-standard instrument and as such calibrated accurately at regular intervals (the details of which are superfluous here); this means, however that the time series is long and reliable. This study uses values of H with 10s time resolution in the interval 1988-2013 inclusive. In contrast to the studies by *Wanliss and Reynolds* [2003] and *Hamid et al.* [2009], here entire years are analysed. Another important difference is the geographical location: at high latitude, most geomagnetic

disturbances occur in the evening sector and the fluctuations in H reflect the rotation of the Earth underneath the auroral oval's typically zonally-aligned current systems which move meridionally backwards and forwards in a sporadic fashion over the magnetometer site. Activity can be expected to repeat at timescales of 1 day, and of course over solar rotation (Carrington rotation) [e.g. *Bartels*, 1934] and longer periods such as the 11-year solar cycle. In order to eliminate these deterministic features from the dataset to be studied a boxcar filter is applied to remove fluctuations less than 24h; the smoothed time-series is then subtracted from the original to arrive at a set of residuals representing the stochastic component. A corresponding method was employed by *Hall* [2014] and discussed and tested by *Hall et al.* [2011]. As will be shown, an advantage of spectral analysis is that individual periodicities remaining in the (supposedly) stochastic residual show up as narrow spikes and in practice have an insignificant influence on determination of the slope of the spectrum. On the contrary, in DFA such periodicities are in general *not* distinguishable.

An example of the input data, in this case for 2001 – in the middle of the overall time interval - is shown in Figure 1. The top panel shows the original data in black and with a 1-day smoothing superimposed. The bottom panel zooms in on 1st June 2001 and shows the result of subtracting the smoothed time series from the original to obtain a residual representing the stochastic component. In addition, the smoothed data are shown with mean subtracted corresponding to the upper panel. As will be demonstrated forthwith, the removal of the 1-day running mean did not affect the non-stationarity of the signal at shorter timescales. Other years are similar. In Figure 2., the top panels show the distribution of the stochastic component with linear (left) and logarithmic (right) ordinates, again from 2001. In a somewhat unsophisticated approach, although adequate to the purpose, the maximum of the distribution and its width at half-maximum are determined. The mean is assumed to be zero

165 as a result of the subtraction of the deterministic component as illustrated in Figure 1. Corresponding Gaussian and Cauchy distributions are determined and these are also shown in the figure. A characteristic of the distributions (for all years) is that they are skewed; this is because the current in the overlying ionosphere tends to have a preferred orientation and perturbations of the horizontal geomagnetic field tend to be negative on average.

170 Qualitatively the Cauchy distribution is a better description of that of the data than the Gaussian. Again all years are similar, although for less skewed distributions the suitability of the Cauchy model is even more evident. Furthermore, in contrast to the Gaussian model the data exhibit heavy tails. The bottom panels of Figure 2. show the quantile-quantile (Q-Q) portrayals – left: vs. Gaussian and right: vs. Cauchy. The departures from linearity (i.e. in the

175 central regions of the respective plots) are indicative of long tails at both ends of the distribution relative to the model. See *Chambers et al.* [1963] for diagnostics of Q-Q plots. The Cauchy distribution reproduces the tails in the data distribution rather better than the Gaussian. Recall, however that in this simple approach, the half-maximum full-width values have been matched and comparisons might have been improved by choosing $1/e$ or another

180 arbitrary value. Nonetheless, a Cauchy distribution would always represent the tails in the data distribution better than a Gaussian. It is important to note at this point that a Cauchy process can be defined as a Brownian motion subordinated to a process associated with a Lévy distribution [*Sato*, 1999]. Again, it should be noted that analyses for all 25 years exhibit similar characteristics, and thus that the results hitherto justify the further investigation that

185 follows.

The next step is to determine the power spectral density and its scaling with respect to frequency. As stated earlier it is incorrect to presuppose there are no data breaks and therefore a Lomb-Scargle periodogram is derived, rather than the more traditional Fourier transform,

but having first preconditioned the time series by applying a parabolic window and bridge
 190 detrending using the first and last points. The result (again for 2001) is shown in the left panel
 of Figure 3. At periods greater than one day fluctuations have been effectively removed by
 the subtraction of the deterministic component, and, as predicted, discrete peaks at one-day
 and (approximately) 12h remain demonstrating the method not to be perfect. Vertical dotted
 and dashed lines indicate familiar timescales. Convincing scaling is evident from 1 day down
 195 to approximately 5 min; there is a suggestion of a subrange between 5 and 1-minute scales
 and then a tendency to flattening. The scaling exponent β has therefore been obtained over
 two subranges, day-minute and 12h-1h indicated on the plot by red ($\beta = 2.014 \pm 0.001$) and
 cyan ($\beta = 1.811 \pm 0.012$) lines respectively. The annotation gives the result of the overall day-
 minute scaling (the red line) expressed as the generalized Hurst exponent α (1.51), whereas
 200 the 12h-1h scaling yields $\alpha = 1.41$. The DFA(1) analysis of the same data is shown in the
 right hand panel of Figure 3. The interval for the linear fit is chosen as a result of examination
 of the spectrum and with an a priori knowledge of the behaviour of the geomagnetic
 component. Again familiar timescales are indicated in the plot, and linearity over
 approximately 2 orders of magnitude yields $\beta = 1.474 \pm 0.002$. This linearity starts around 10
 205 minutes (from inspection of the figure), however the density of points is low at the small-
 timescale region (the plot being logarithmic) such that the fitting of the straight line is
 essentially unaffected by including points between 1 and ~10 min. The linearity weakens
 after about 12 hours when the curve begins to flatten (as could be anticipated from inspection
 of the spectrum). Departure from the fitted line is easy to identify at longer timescales, but
 210 not at shorter timescales, as opposed to as seen in the SA approach. On the other hand, DFA
 results in a much “cleaner” plot that in turn is conducive to deceptively reliable linear fitting.
 Had timescales $> 1h$ been excluded from the fit in the DFA, α from the overall SA and α from
 the DFA would have been similar. It can be argued that SA is easier to interpret because a

physicist would normally have some preconception of the processes characterized by
215 different timescales, hidden to some degree when using only DFA. The SA method is
preferred here because of closer contact with any underlying physics and reliability of
identification of different subranges for linear fitting. At this point the method used here
departs somewhat from that used by *Hall* [2014], in which surrogate data were generated and
then compared with the original [*Theiler et al.* 1992]. For the purposes of this study, at least,
220 generation of, for example 100 surrogate data sets corresponding to 1-year long 10s
resolution (i.e. over 3 million points) followed by DFA analyses is not practicable for
computational reasons. Inspection of the probability distribution functions combined with
visual comparison with known distributions and subsequently Q-Q analyses is deemed to
confirm the complex nature of the stochastic process in the data. Again, only one year's
225 results are shown here; all 25 years exhibit similar values of α when for each of DFA and the
two SA subranges.

The results of analysing all 25 years from 1988 to 2013 inclusive as described and illustrated
for 2001 above are shown in Figure 4. From top to bottom the panels show: DFA(1), SA (1d–
1min) and SA (12h-1h). The final panel shows yearly mean sunspot numbers from the Solar
230 Influence Data Analysis Center (SIDC) [*Clette*, 2011]. For each year (small) vertical bars
indicate the $1-\sigma$ uncertainty in the individual linear fits. It is evident (by comparing axes) that
by taking all scales between 1d and 1min in the SA, α is always > 1.5 . DFA and SA (12h-1h)
the α s are similar and always < 1.5 . There are considerable year-to-year variations
irrespective of method, but no obvious periodicity that could be attributable to the two solar
235 cycles the data set spans. On the other hand, linear regressions reveal trends, which are also
indicated in the figure together with 95% confidence limits according to the method of
Working and Hotelling [1929]. The trends are small but worth mentioning here to give the

possibility for comparison with other studies in future. For DFA the trend is 0.04 ± 0.05 century⁻¹; for SA (1d-1min), 0.2 ± 0.2 century⁻¹; for SA (12-1h), 0.01 ± 0.1 century⁻¹. Since
 240 in all 3 cases, the uncertainties are approximately equal to the trends themselves, none of the values can be considered to be significant. The mean values of α over the 25 years are: DFA, 1.46 ± 0.02 ; SA (12h-1h), 1.54 ± 0.07 ; SA (1d-1min), 1.39 ± 0.04 .

Discussion

To summarize the above findings, all analyses, irrespective of scale, indicate fBm. Both SA
 245 used in the regime 12h - 1h and DFA (in which determination of the scaling exponent is weighted towards the longest scales), indicate $\alpha \approx 1.42$. For day-minute scales SA yields $\alpha = 1.54$ but the uncertainty dictates that the result cannot be regarded as significantly different from, for example that of the DFA. The results weighted towards longer timescale fluctuations, however, exhibit small enough uncertainties that taken collectively one can
 250 conclude that α is slightly less than 1.5, the significance of which will be discussed forthwith. Other studies of complexity in geomagnetic, or geomagnetically related time series have either used isolated periods of, for example, months [Wanliss and Reynolds, 2003; Hamid et al., 2009] albeit with time resolution comparable to that used here, or much longer derived datasets of, for example AE-index with different time resolution. Rypdal and Rypdal [2010]
 255 studied AE-index at timescales similar to those addressed here. Obtaining a synthesis, even over several relatively local time-series (as is done when determining the AE index, but especially globally – e.g. for the KP index) will tend to even out variances over intra-diurnal timescales, e.g. occurrence of local ionospheric current systems. Any non-stationarities may be masked out such that local determinations of α and identification of processes as fGn or
 260 fBm may well differ. Wanliss and Reynolds [2003] and Hamid et al. [2009] employed geomagnetic data from specific stations, but for low latitude. In contrast to the analyses here,

Wanliss and Reynolds [2003] examined only a short time interval of 5 days, but for 6 different Southern Hemisphere sites determining α to increase approximately with increasing latitude (southward) from $\alpha = 1.55$ to $\alpha = 1.69$ i.e. fBm but with consistently slightly higher exponents than determined here. *Hamid et al.* [2009] employed a longer dataset (1 month) than *Wanliss and Reynolds* [2003] but for 2 sites. However *Hamid et al.* [2009] categorized days as active or quiet and finding active days exhibited $\alpha = 1.64$ and 1.55 for the two sites, and, for quiet days, $\alpha = 1.45$ and 1.33 . In this study, no attempt has been made to pick out quiet and disturbed days. Over the course of an entire year, however, it could be expected that quiet days predominate considering that the rapid perturbations extracted from the observation and deemed to be a stochastic component rely on current systems being approximately over the magnetometer. The findings in this study, viz. that α lies slightly under 1.5, can be considered in good agreement with those of *Wanliss and Reynolds* [2003] and *Hamid et al.* [2009]. In order to attempt to discriminate between active and quiet years [e.g. *Vaquero et al.*, 2014], however annual mean sunspot numbers have been plotted in the bottom panel of Figure 4. There is no conclusive correlation between solar activity and the values of α from the 2 methods (and 2 scaling ranges). If the trends could be considered significant (which they are not) they might be seen to anticorrelate with overall solar activity over the 25 years (quieter sun) which would contradict the suggestion by *Hamid et al.* [2009] that active days are characterized by $\alpha > 1.5$.

Wanliss and Reynolds [2003] point to several publications employing high latitude geomagnetic data, but these use the *AE* index. *Takalo et al.* [1994] find that *AE* scales with $\alpha \approx 1$ for low frequencies (timescales > 100 min) and $\alpha \approx 1.5$ for high frequencies (1-100 min, and therefore shorter than typical substorm durations). Note that *Takalo et al.* [1994] use “ α ” for power-law dependence whereas this study uses “ β ”, and thereafter *Rypdal and Rypdal*

[2010] convert *Takalo et al.*'s value to “ H ” – the Hurst exponent. In terms of the classification used here and also by *Kantelhardt et al.* [2006], AE appears as a non-stationary process for intra-sub-storm timescales with $\alpha \approx 1.5$ but becoming stationary (i.e. fGn) when only $>$ sub-storm timescales are considered. This is compatible with the findings here
 290 because at any given instant, it is unlikely that the same geomagnetic fluctuations will be registered by more than a few geographically grouped observations: AE and the stochastic component of H should be expected to exhibit similar signatures at short timescales, and this is the case here.

Other studies of geomagnetic signatures include analysis of the Disturbance storm time (Dst)
 295 index, e.g. by *Balasis et al.* [2006], who calculate, explicitly, β for periods during 2001 and for the entire year. Scaling was examined in the range 5d-2h and indicated α between ~ 1.4 and ~ 1.6 . However inspection of the spectra, and particularly for the whole year (as used here too) there is a suggestion of a change of slope at ~ 10 h, such the higher frequency subrange would yield a slightly higher (presumably > 1.5) result for α . This is not the same as the
 300 spectral breakpoint mentioned in this study, but together they illustrate that bicoloured noise [*Takalo et al.*, 1994] may well be present. Recent exploits into comparing complexity signatures are worthy of note: *Scafetta and West* [2003] proposed terrestrial temperature anomalies to be linked to solar flare intermittency via a Lévy process. *Rypdal and Rypdal* [2011] find identical multifractal noise signatures in both the AE index and the z-component
 305 of the interplanetary magnetic field suggestive of the existence of mechanisms linking intermittency in the two. These studies utilised very long datasets, typically of 1-month time resolution aimed at facilitating better trend analyses and prediction of future climate, Here, similar techniques are employed on shorter (\sim years) datasets with higher time resolution (\sim seconds) but to help identify differences between geographically local complexity.

310 *Kantelhardt et al.* [2006], using different hydrological data types, explain how results from shorter-term data could be modelled by an autoregressive moving-average (ARMA) [Wittle, 1951], but given the time series lengths and similarities with other work, fBm seems a good candidate to model the stochastic nature of the geomagnetic field.

Conclusions

315 To conclude: 25 years of 10s local measurements of the horizontal component of the geomagnetic field are examined, one year at a time. All variability with timescales 1-d or longer thus including anticipated and/or known periodicities are removed. This is analogous to deseasonalization of, for example, monthly temperature data – a common practice for meteorological time-series, but apparently not necessarily the case, nor meaningful, for
320 studies of the *AE* index. Thereafter, quantile-quantile (Q-Q) followed by spectral and detrended fluctuation analyses (SA and DFA respectively) are performed revealing, as a characteristic common to all years, distributions better described as Cauchy rather than Gaussian. The SA, performed here by a Lomb-Scargle periodogram analysis, rather than the more usual Fourier analysis, in order to allow for data-gaps, suggests bicoloured spectra,
325 more difficult to discern if using DFA alone. The resulting generalized Hurst exponents, α , all lie in the region of 1.5 (mostly ≈ 1.42), although there is a possibility that for shorter timescales (down to 1 min) $\alpha \approx 1.55$. The former is indicative of fractional Brownian motion (fBm) but with a degree of likelihood for fast switching of direction in the motion (antipersistence), while the latter is indicative of a higher persistence. This difference could
330 be explained thus: during the course of an evening, changes in the position of the auroral electrojet can be considered rapid, whereas from minute-to-minute the electrojet moves more persistently in geomagnetic latitude. The results are in excellent agreement with independent findings both derived from local data, as used here, and with zonally synthesized data as

comprises the *AE* index, for example. In particular, *Takalo and Timonen* [1994] identified
335 two subranges in the power spectrum of *AE*, attributing the lower frequency regime to
turbulence in the solar wind and the higher frequencies to origins in the magnetosphere. This
would, in addition, support a hypothesis that geomagnetic field variations can be universally
described by fractional Brownian motion. Matching this signature with those identified in
space weather parameterizations add to a growing arsenal of tools available for understanding
340 and forecasting the impact of solar activity on the terrestrial environment. This study also
points the way to further, although computationally demanding, analyses including use of
geomagnetic data from other locations, hypothesis-testing using surrogates and more refined
data selection according to disturbed conditions.

345 **Acknowledgements.** The author acknowledges the staff of Tromsø Geophysical Observatory
for ensuring consistency in the dataset chosen for this study and in particular Børre Heitmann
Holmeslet for assistance in assembling the time series. Data from the Tromsø station can be
obtained via World Data Centres for Geomagnetism.

350 **References**

- Balasis, G., I.A. Daglis, P. Kapisiris, D. Vassiliadis and K. Eftaxias (2006), From pre-storm activity to magnetic storms: a transition described in terms of fractal dynamics, *Ann. Geophys.*, 24, 3557-3567.
- Bartels, J. (1934), Twenty-Seven Day Recurrences in Terrestrial-Magnetic and Solar
355 Activity, 1923-1933, *Terrestrial Magnetism and Atmospheric Electricity* 39 (3): 201–202.
- Bartels, J., N.H. Heck and H.F. Johnston (1939). The three-hour range index measuring geomagnetic activity, *Geophys. Res.*, 44, 411-454
- Chambers, J.M., W.S. Cleveland, B. Kleiner and P.A. Tukey (1963). *Graphical Methods for Data Analysis*. 395pp., Duxbury Press, Boston, Massachusetts.
- 360 Clette, F. (2011), Past and future sunspot indices: new goals for SoTerIA, *J. Atmos. Sol.-Terr. Phys.*, 73, 182–186.
- Davis, T.N., and M. Sugiura (1966), Auroral electrojet activity index AE and its universal time variations, *J. Geophys. Res.*, 71, 785-801.
- Delignieres, D., S. Ramdani, L. Lemoine, K. Torre, M. Fortes and G. Ninot (2006), Fractal
365 analyses for ‘short’ time series: A re-assessment of classical methods, *J. Mathematical Psychology*, 50, 525-544.
- Eichner, J.F., E. Koscielny-Bunde, A. Bunde, S. Havlin and H.-J. Schnellhuber (2003), Power-law persistence and trends in the atmosphere: A detailed study of long temperature records, *Phys. Rev. E*, 68, 046133.

- 370 Eke, A.H., P. Hermán, J. B. Bassingthwaite, G. M. Raymond, D. B. Percival, M. Cannon,
I. Balla, and C. Ikrényi (2000), Physiological time series: Distinguishing fractal noises
from motions, *Pfügers Archives*, 439, 403-415.
- Fougère, P.F. (1985), On the accuracy of spectrum analysis of red noise processes using
maximum entropy and periodograms methods: Simulation studies and application to
375 geographical data, *J. Geographical Res.*, 90(A5), 4355-4366.
- Grassberger, P., and I. Procaccia (1983), Measuring the strangeness of strange attractors,
Physica D, 9(1-2), 189-208.
- Hall, C.M., K. Rypdal and M. Rypdal, (2011) The E-region at 69°N 19°E: trends,
significances and detectability, *J. Geophys Res.*, 116, A05309, doi:
380 10.1029/2011JA016431.
- Hall, C.M. (2014), Complexity signatures for short time scales in the atmosphere above
Adventdalen, Svalbard, *J. Geophys. Res. Atmos.*, 119, doi:10.1002/2013JD020988.
- Hamid, N.S.A., G. Gopir, M. Ismail, N. Misran, A.M. Hasbi, M.D. Usang and K. Yumoto
(2009), The Hurst exponents of the geomagnetic horizontal component during quiet and
385 active periods, *Proc, 2009 Int. Conf. on Space Sci. and Comm.*, 186-189, IEEE publishing,
US and Canada
- Hartmann, A., P. Mukli, Z. Nagy, L. Kocsis and P. Hermán (2013), Real-time fractal signal
processing in the time domain, *Physica A*, 392, 89-102.
- Heneghan, C., and G. McDarby (2000), Establishing the relation between detrended
390 fluctuation analysis and power spectral density analysis for stochastic processes, *Phys. Rev.*
E, 62(5), 6103-6110

- Hurst, H.E. (1951), Long-term storage of reservoirs: an experimental study, *Trans. American Soc. of Civ. Eng.*, *116*, 770-799.
- 395 Kantelhardt, J.W., E. Koscielny-Bunde, D. Rybski, P. Braun, A. Bunde and S. Havlin (2006), Long-term persistence and multifractality of precipitation and river runoff records, *J. Geophys. Res.*, *111*, D01106, doi:10.1029/2005JD005881.
- Koscielny-Bunde, E., A. Bunde, S. Havlin, H.E. Roman, Y. Goldreich and H.-J. Schnellhuber (1998), Analysis of daily temperature fluctuations, *Phys. Rev. Lett.*, *81*(3), 729-732.
- 400 Lennartz, S., and A. Bunde (2009), Trend evaluation in records with long-term memory: application to global warming, *Geophys. Res. Lett.*, *36*, L16706, doi:10.1029/2009GL039516.
- Mandelbrot, B.B., and J.W. van Ness (1968), Fractional Brownian motions, fractional noises and applications, *SIAM Review*, *10*, 422-437.
- 405 Mandelbrot, B.B. (1983). *The fractal geometry of nature*, 486 pp., Macmillan, ISBN 978-0-7167-1186-5.
- Peng, C.K., J. Mietus, J. Hausdorff, S. Havlin, H.E. Stanley and A.L. Goldberger (1993), Long-range anticorrelations and non-Gaussian behavior of the heartbeat, *Phys. Rev. Lett.*, *70*, 1343-1346.
- 410 Press, W.H., and G.B. Rybicki (1989), Fast algorithm for spectral analysis of unevenly sampled data, *The Astronomical J.*, *338*, 277-280.
- Rishbeth, H. and M. Clilverd (1999), Long-term change in the upper atmosphere, *Astronomy and Geophysics*, *40*, 3.26-3.28.

- Roble, R.G. and R.E. Dickinson (1989), How will changes in carbon-dioxide and methane
415 modify the mean structure of the mesosphere and thermosphere? *Geophys. Res. Lett.*, *16*,
1441-1444.
- Rypdal, M., and K. Rypdal (2010), Stochastic modeling of the AE index and its relation to
fluctuations in B_z of the IMF on time scales shorter than substorm duration, *J. Geophys.*
Res., *115*, A11216, doi:10.1029/2010JA015463.
- 420 Rypdal, M., and K. Rypdal (2011), Discerning a linkage between solar wind turbulence and
ionospheric dissipation by a method of confined multifractal motions, *J. Geophys. Res.*,
116, A02202, doi:10.1029/2010JA015907.
- K. Sato (1999), Lévy processes and infinitely divisible distributions, *Cambridge*
Studies in Advanced Mathematics, *68*, Cambridge University Press, Cambridge.
- 425 Scafetta, N., and B.J. West (2003), Solar flare intermittency and the Earth's temperature
anomalies, *Phys. Rev. Lett.*, *90*(24), 248701, doi: 10.1103/PhysRevLett.90.248701.
- Takalo, J., and J. Timonen (1994), Characteristic timescale of auroral electrojet data,
Geophys. Res. Lett., *21*, 617-620.
- Takalo, J., J. Timonen and H. Koskinen (1994), Properties of AE data and bicolored noise, *J.*
430 *Geophys. Res.*, *99*, A7, 13,239-13,249.
- Theiler, J., S. Eubank, A. Longtin, B. Galdrikian and J.D. Farmer (1992), Testing for
nonlinearity in time series: the method of surrogate data, *Physica D*, *58*, 77-94.
- Vaquero, J.M., S. Gutiérrez-López and A. Szelecka (2014), A note on the relationship
between sunspot numbers and active days, *Adv. Space Res.*, *53*(8), 1180-1183.

435 Vasseur, D.A., and P. Yodzis (2004), The color of environmental noise, *Ecology*, 84(4),
1146-1152.

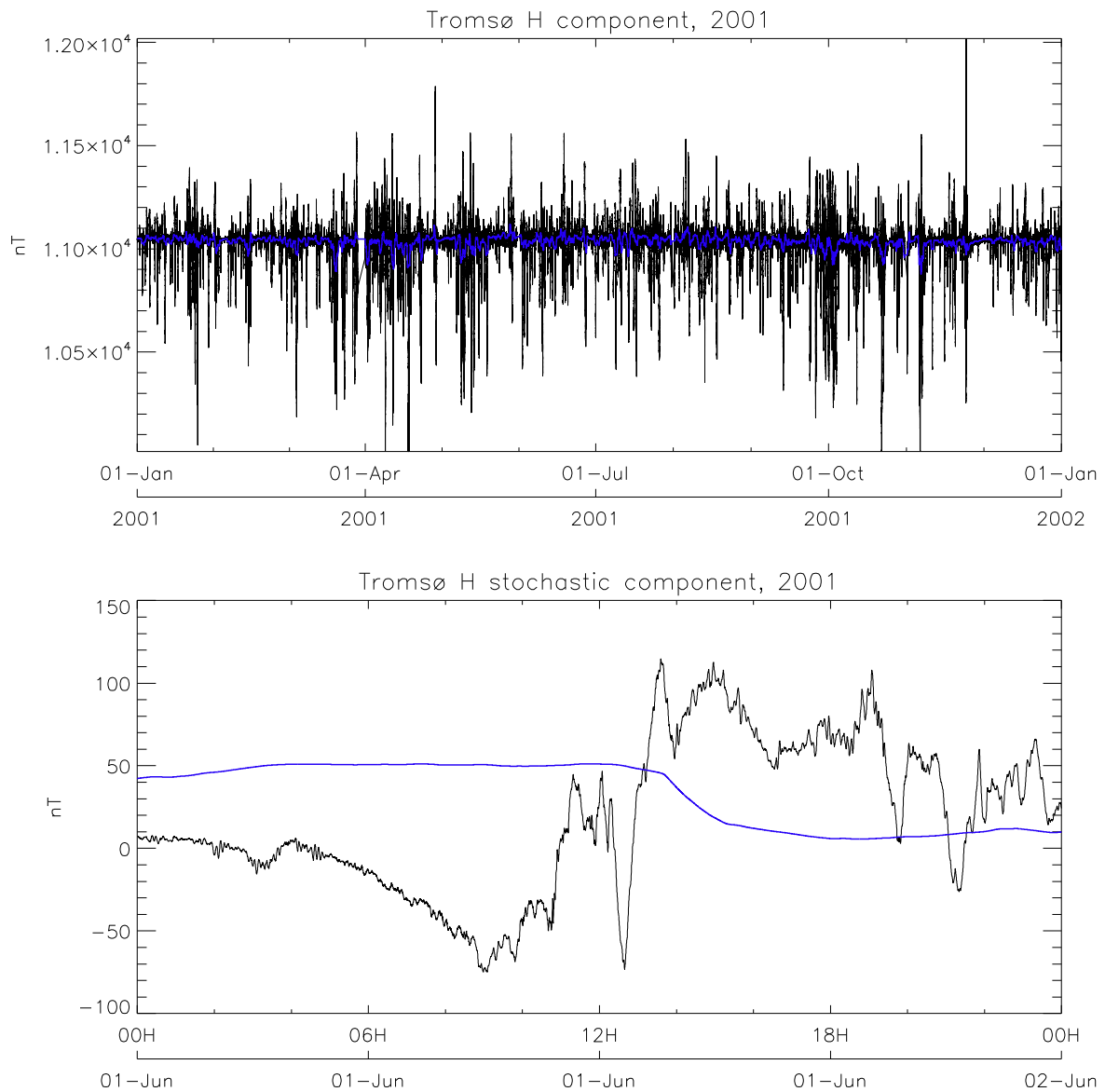
Wanliss, J.A., and M.A. Reynolds (2003), Measurement of the stochasticity of low-latitude
geomagnetic temporal variations, *Ann. Geo.*, 21, 2025-2030.

Wilk, M.B., R. Gnanadesikan (1968), Probability plotting methods for the analysis of data,
440 *Biometrika* (Biometrika Trust) 55 (1): 1–17

Whittle, P. (1951), *Hypothesis Testing in Time Series Analysis*, 120pp, Hafner Publishing
Co., New York.

Working, H., and H. Hotelling (1929), Application of the theory of error to the interpretation
of trends, *Journal of the American Statistical Association*, 24, 73–85.

445



450 Fig. 1. H-component of geomagnetic field from Tromsø, 70°N, 19°E for the year 2001. Data are at 10s time resolution. The top panel shows the original data in black and with a 1-day smoothing superimposed in blue. The bottom panel shows a detail of the residual - the result of subtracting the smoothed time series from the original - for 1st June, and with the mean-subtracted 1-day smoothing, again superimposed in blue.

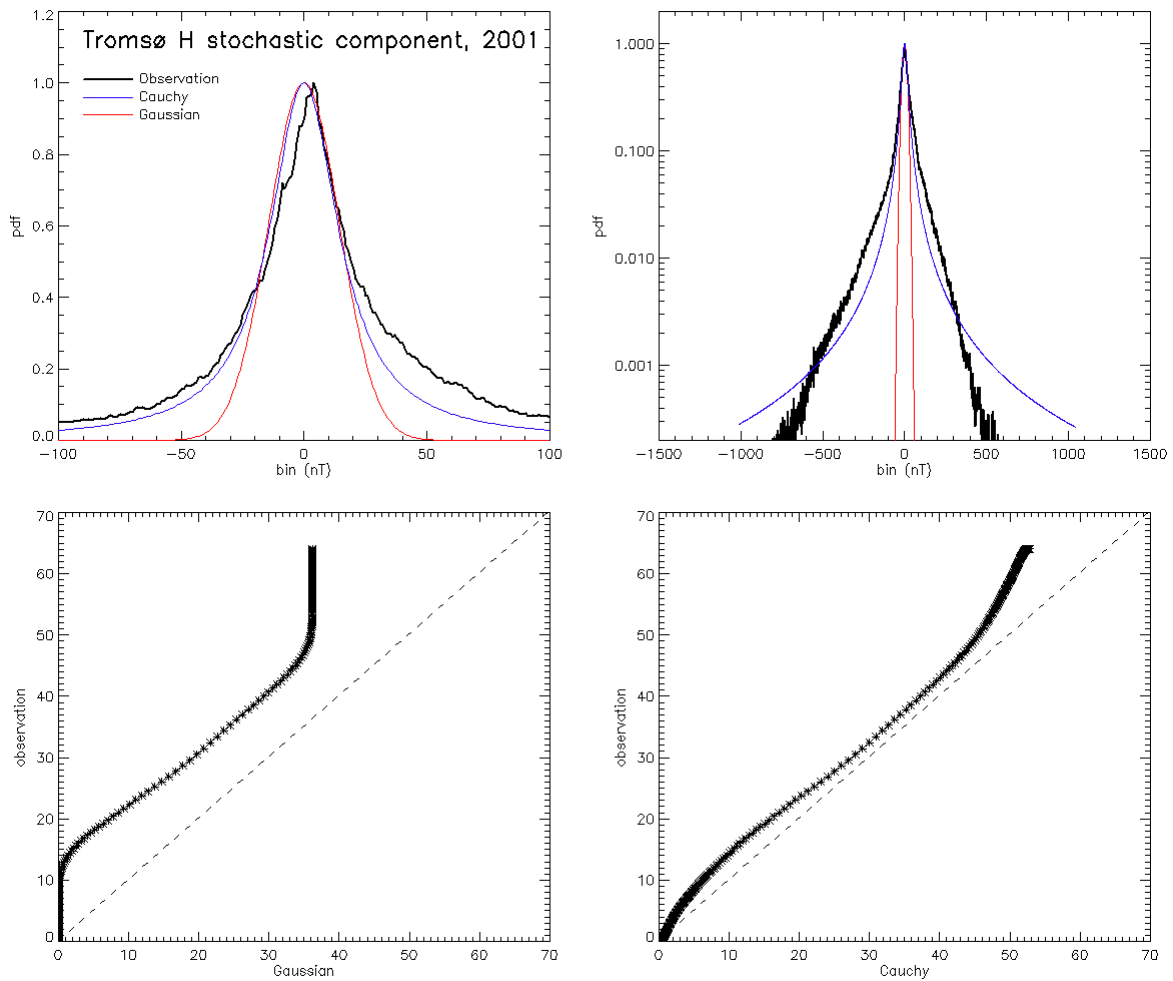


Fig. 2. Portrayals of the distribution of the stochastic component of the H-component of the geomagnetic field from 2001 as shown in Figure 1. Top-left: linear ordinate axis; top right: logarithmic ordinate axis. In the top panels Gaussian (red) and Cauchy (blue) distributions are fitted (explained and discussed in the text). Bottom left: Q-Q plot of the observed data versus Gaussian; bottom right: Q-Q plot of the observed data versus Cauchy.

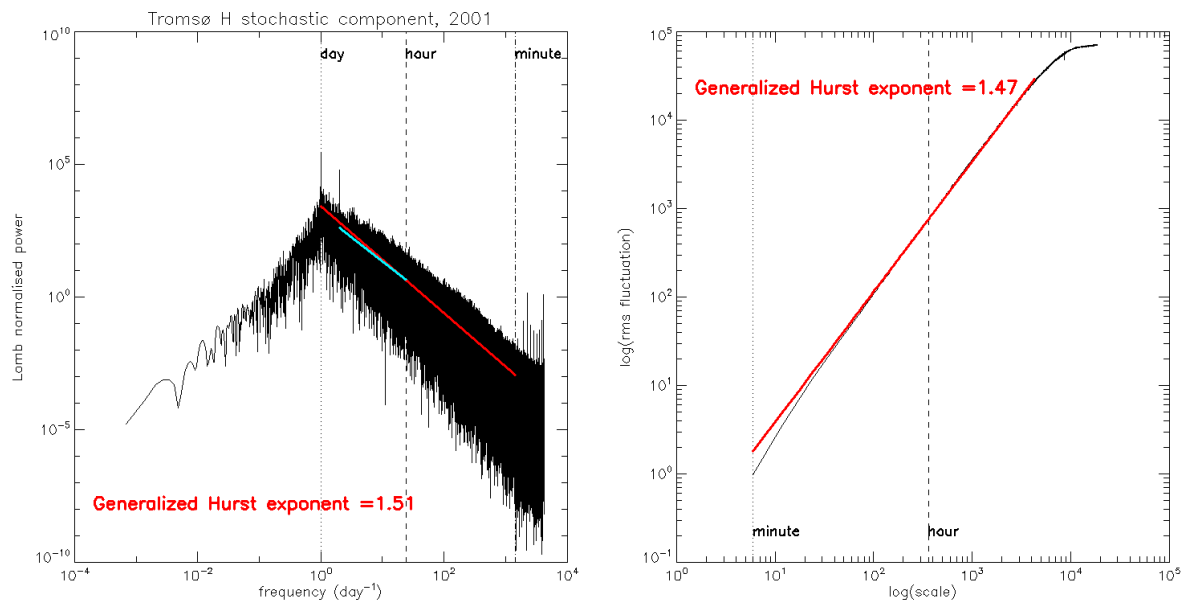
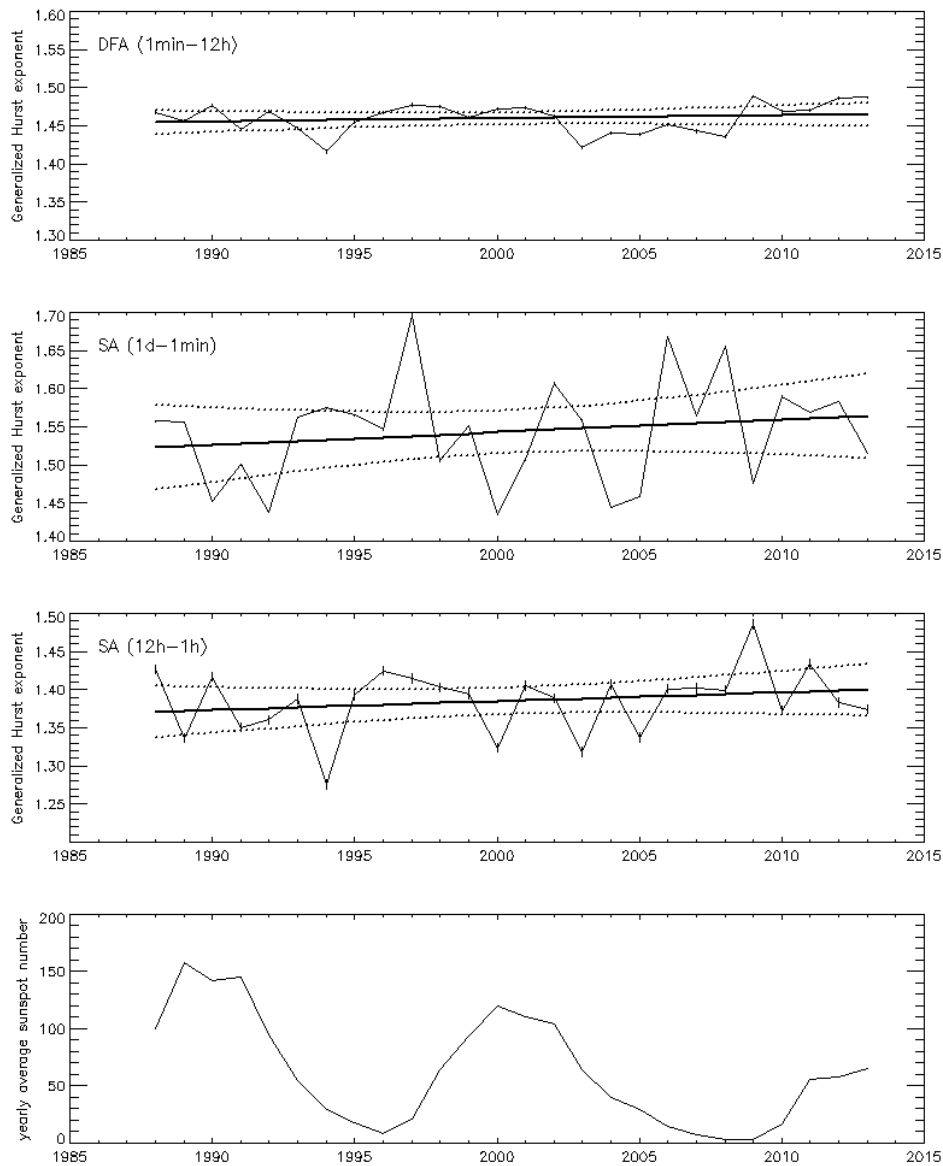


Fig. 3. Spectral (left) and detrended fluctuation (right) analyses for data shown in previous figures. Familiar timescales are indicated by vertical dotted/dashed lines. Fitted scaling exponents are shown by coloured lines together with corresponding values.



475 Fig. 4. Generalized Hurst exponents (β) from all years 1988-2013 (with uncertainties). Top: DFA method; second panel: SA method using range 1 day-1 min.; third panel: SA using only 12h-1h. Tentative linear trends are shown together with 95% confidence limits indicated by dotted hyperbolae. Bottom panel: yearly average sunspot numbers.